RSC Advances

PAPER

View Article Online
View Journal | View Issue

Cite this: RSC Adv., 2016, 6, 27205

The effect of barium sulfate-doped lead oxide as a positive active material on the performance of lead acid batteries†

Xiqing Yuan,‡ Jingping Hu,‡ Jingyi Xu, Yucheng Hu, Wei Zhang, Jinxin Dong, Sha Liang, Huijie Hou, Xu Wu and Jiakuan Yang*

Received 21st January 2016
Accepted 4th March 2016

DOI: 10.1039/c6ra01873d

www.rsc.org/advances

Barium sulfate ($BaSO_4$) is a common impurity in recycled lead paste that is challenging to eliminate completely during hydrometallurgical recycling of spent lead acid batteries, so the effect of this impurity in positive active materials on the performance of recycled lead acid batteries was investigated. The $BaSO_4$ doped lead oxide composite was used as a positive active material in positive plates of lead acid batteries with theoretical capacities of 2.0 A h. $BaSO_4$ was retained in the solid phase throughout the battery fabrication process. Different $BaSO_4$ dosages affected the phase of the positive plates during the curing process, with the highest content of metallic lead obtained at a $BaSO_4$ dosage of 0.06 wt%. Morphology analysis indicated that aggregates were formed in the positive plates and the particles became rougher with increasing addition of $BaSO_4$ during the formation process. $BaSO_4$ also demonstrated a large impact on charge/discharge cycles with 100% DOD in battery testing. Analysis of disassembled failed batteries indicated that the expansion and shedding-off of the positive active material were mainly responsible for the failure of these batteries, and this could be attributed to the non-uniform growth of lead oxide on the $BaSO_4$ nucleus, and the accumulation of internal stress.

1 Introduction

Lead–acid batteries have been extensively utilized in electric bicycles,[1] energy storage[2–5] and many other applications[6] over the last few decades. They account for about fifty percent of the battery market.[7,8] However, the lead–acid battery industry faces many serious challenges with the development of the energy industry.[9] Besides the issue with relatively low theoretical mass capacity and limited utilization of the active mass of lead–acid batteries, the green recovery of spent lead paste is also a big challenge during the recovery of waste lead acid batteries.

Two recovery methods of spent lead paste have been widely studied,[10] including traditional pyrometallurgical and alternative hydrometallurgical processes. Traditional pyrometallurgical process could have barium sulfate ($BaSO_4$) easily removed from final lead ingot product, however, it is largely criticized due to serious emission of SO_2 and release of lead dust to the environment.[11] In contrast, hydrometallurgical process has been studied recently as an alternative method for spent lead paste recovery without emission of hazard gases and lead particulates,[12] but it couldn't eliminate $BaSO_4$ component completely. Pan *et al.* proposed a green lead hydrometallurgical process based on a hydrogen–lead oxide fuel cell,[13] and demonstrated a new green hydrometallurgical process to recover lead based on this fuel cell, and lead and electricity were produced together with water as the only by-product. Nano-structured lead oxide product was synthesized by calcination of lead citrate precursor recovered from spent lead paste *via* novel hydrometallurgical process.[14] Removal of impurities from the recovered product is a common challenge in the hydrometallurgical process. When lead oxide products recovered from spent lead paste was re-used as active materials for new lead–acid battery fabrication, $BaSO_4$ inevitably existed in both positive active materials (PAM) and negative active materials (NAM). Studies on synthesized leady oxide for PAM of lead acid battery showed low capacity retention ratio[15,16] and the existence of $BaSO_4$ were mainly responsible for the poor capacity retention ratio. So, it is inspiring to investigate the effect of $BaSO_4$ impurities in lead oxide as PAM on the performance of lead–acid battery.

Many additives, such as $BaSO_4$, acetylene black, lignosulfonates, have been used in NAM on the negative plate in order to improve the utilization of active mass and cycle stability in lead–acid battery. $BaSO_4$ can be used as bulking agent and has been intensively studied as a common additive of negative plate in the lead–acid battery. It has been shown that $BaSO_4$ lowered the overpotential of $PbSO_4$ nucleation,[17] or served as seed crystals for

School of Environmental Science and Engineering, Huazhong University of Science and Technology (HUST), Wuhan, 430074, P. R. China. E-mail: jkyang@hust.edu.cn; yjiakuan@hotmail.com; Fax: +86-27-87792101; Tel: +86-27-87792207

† Electronic supplementary information (ESI) available: see DOI: 10.1039/c6ra01873d

‡ These two authors contributed equally to this paper.

the precipitation of $PbSO_4$.[18] However, when lignosulfonates and $BaSO_4$ were utilized as negative plate additives, they have demonstrated to improve the reversibility during the charge–discharge process in the high-rate partial-state-of-charge (HRPSoC) mode and prolong the cycle life time.[17] The effect of particles size variation of $BaSO_4$ was also investigated when used as additive for the negative plate,[19] and no influence on the cycle-life performance of cells under HRPSoC condition was observed. The effect of $BaSO_4$ and $SrSO_4$ was investigated as seed crystals by electrochemical atomic force microscopy (AFM).[20] $PbSO_4$ crystals were formed more rapidly on $SrSO_4$ than on $BaSO_4$ during the discharge process. Electrochemical reactions on negative plate were also investigated using electrochemical AFM to explore the mechanisms of oxidation and reduction on the lead/sulphuric acid interface when barium sulfate was added to the negative plate in the lead–acid battery,[18] and the result indicated that $BaSO_4$ provided nucleation seeds for the formation of $PbSO_4$ crystallites. However, there is few reports on the effect of $BaSO_4$ as additive for positive plate on the performance of battery. The effect of $BaSO_4$ as additive in the electrolyte for the electrochemical deposition of leady dioxide was studied, and cyclic voltammetry and battery testing results showed that $BaSO_4$ with concentration of 10^{-5} M could be used as suitable electrolyte additive to improve the performance of the battery,[21] but the effect of $BaSO_4$ as solid additive to the positive plate was still not clear when the plate was prepared through the commercial battery manufacturing process.

In this work, we studied the effect of $BaSO_4$ impurity in PAM on the performance of lead acid battery and investigated the impact on the change of morphology and crystal structure of the plate during the whole battery production process.

2 Experimental

2.1 Materials and chemicals

Simulated spent lead paste (comprising $PbSO_4$, PbO_2, PbO, and metallic Pb) was prepared by mixing analytical reagents according to the chemical composition of spent lead paste in spent/discarded lead acid battery, as shown in Table S2.† Synthesized lead oxide was prepared following the method in the literature.[14] The solution of sodium citrate and acetic acid were utilized as leaching reagents. Hydrogen peroxide was used as a reduction reagent to reduce lead dioxide to lead monoxide. The lead citrate precursor was firstly synthesized from simulated spent lead paste *via* hydrometallical process. And then novel ultrafine lead oxide products were prepared by the calcination of lead citrate precursor at 375 °C which was much lower than typical temperature used in pyrometallurgical process. Sodium citrate ($Na_3C_6H_5O_7 \cdot 2H_2O$, 99 wt%), acetic acid ($CH_3COOH$, 99.5%), hydrogen peroxide (H_2O_2, 30%), $BaSO_4$ (99 wt%) and concentrated sulfuric acid (98% purity) were obtained from Sino-pharmaceutical company of China.

2.2 Barium sulfate addition and measurement

The solid phase powder was mixed with synthesized lead oxide (100 g) with different mass dosage of $BaSO_4$ (0.02 wt%, 0.04 wt%, 0.06 wt%, 0.08 wt%, 0.1 wt%) by grinding in a mortar for 40 min. These concentrations were selected according to the typical $BaSO_4$ concentration found in recycled spent lead paste (0.05–0.1 wt%). The concentration of barium ion in the solution was measured by Inductively Coupled Plasma (Optima 8300, PerkinElmer, US) after digesting 0.2 g sample with 15 mL boiled *aqua regia*.

2.3 Electrochemical study of lead oxide

Detailed procedures for the preparation of working electrode (WE) for the electrochemical study are provided as follows. Firstly, lead oxide, carbon black and PVDF were mixed according to the mass ratio of 9 : 1 : 1 in the mortar, followed by grinding using pestle and mortar for about 30 minutes, and then mixed with NMP to prepare a homogeneous slurry. Then the resulting paste was transferred onto the surface of a glassy carbon electrode, followed by drying in an oven at 60 °C for 24 hours. Cyclic voltammetry (CV) was carried out using a CHI660E electrochemical workstation (Shanghai Chenhua Instruments Co. Ltd., China). The CV curves of lead oxide were acquired at a scan rate of 10 mV s^{-1} in 3 mol L^{-1} sulfuric acid in a typical three-electrode system, with a lead oxide sample loaded glassy carbon electrode (GCE) as working electrode (WE), a platinum wire as counter electrode (CE), and a $Hg/Hg_2SO_4/K_2SO_4$(sat.) reference electrode (RE).

2.4 Battery assembly, testing and dismantling

The preparation procedure of the positive plate, assembly and testing of the battery have been described previously in the literature.[15] The positive plates (39.5 mm × 65.6 mm) for designed 2 A h testing battery were produced by standard battery assembly process including paste mixing, curing, formation, washing and drying treatment. The nominal capacity of the assembled battery was determined by the depth of discharge, DOD = 100%. After about 47 charge/discharge cycles, the batteries were dismantled after the final charging procedure. The dismantled positive plate was washed in distilled water to remove excess electrolyte on the surface and dried in an oven at 75 °C for 24 h.

The positive paste was scrapped after dismantled, and the compositions of $PbSO_4$ and PbO_2 were measured: 0.2 g sample was screened by the 120 mesh sieve, mixed and sonicated with 10 mL 58.86 wt% HNO_3 and 6 mL 0.83 wt% H_2O_2 separately, and mixed with potassium permanganate ($C = 0.15$ mol L^{-1}) to titration the solution to pink color to determine the amount of residual H_2O_2. The electrolyte acid density was measured by the gravimetric method. The carbon and sulfur composition were measured by frequency infrared carbon and sulfur analyzer (HCS140, Shanghai).

2.5 XRD analysis and SEM analysis

The crystalline phases of lead oxide, plates after curing, plates after formation and dismantled pastes in positive plate of testing battery were identified by X-ray diffraction (XRD) analysis (D/MAX 2550, Rigaku, Japan) using Cu K_α radiation ($\lambda =$

1.54 Å), with the operation voltage and current of 40 kV and 300 mA, respectively.

The morphologies of lead oxide, and the positive plates of testing battery were investigated using scanning electron microscopy (SEM, Sirion 200, FEI, Netherland and JEM-2100F, JEOL, Japan) operated at 10 kV after coating the samples with a thin layer of gold to eliminate charging effect.

3 Results and discussion

3.1 Characterization of lead oxides

The crystal structure and morphology of $BaSO_4$-free synthesized lead oxides were investigated, and the XRD patterns of synthesized lead oxide specimens indicated that lead oxide power mainly comprised PbO with trace amount of metallic Pb. In contrary to the conventional lead oxide, the samples prepared from our novel hydrometallurgical method exhibited a porous structure with ultrafine particles which provides larger contact area to facilitate the electrochemical reaction of the active materials to improve the capacity.

The physicochemical characteristics of leady oxides are summarized in Table S3.† The apparent density of synthesized lead oxide was slightly lower than the traditional ball-milled lead oxide, which was provided by Wuhan Changguang Power. Co. Ltd. The oxidizability of lead oxide was around 85%. Owing to the much smaller particle size and higher porosity, the synthesized lead oxide exhibited much higher water absorption value than traditional lead oxide which was beneficial for higher initial discharge capacity.

The electrochemical assessment was carried out in a three-electrode system by potential cycling for 30 times. It showed a decreased oxidation current attributable to oxygen evolution and a decreased reduction peak current with increasing potential cycles. Furthermore, the redox potential difference (0.25 V initially and 0.15 V after 30 cycles) also became smaller with the potential cycles.

3.2 The effect of $BaSO_4$ on the curing of positive plate

The ultrafine lead oxide was used as PAM, and the prepared positive plate was cured at high temperature. The XRD patterns of PAM specimens after curing are presented in Fig. 1. In this figure, 4BS refers to the $4PbO \cdot PbSO_4$ and 3BS refers to $3PbO \cdot PbSO_4$, which were formed during curing process. 4BS and 3BS would transform to β-PbO_2 and α-PbO_2 respectively in the subsequent formation process, and the former contributed to the initial capacity and the latter contributed to the cycle stability for the batteries. The weak peaks presented in Fig. 1 were attributable to unlabeled peaks from the lead paste. The peak intensity of 4BS at 27.7° was 350 counts in the absence of $BaSO_4$, and increased to 1521 with increasing dosage of $BaSO_4$ to 0.1%. This indicated that the portion of 4BS phase increased with the increasing dosage of $BaSO_4$. The increased ratio of 4BS phase with the addition of $BaSO_4$ can be attributed to the high nucleation density of 4BS on the $BaSO_4$ crystal nucleus.[13] Nevertheless, the content of 4BS did not increase much when the dosage of $BaSO_4$ is 0.1 wt% in contrast to the case of 0.08 wt%. The peaks of $BaSO_4$ became evident for samples with the dosage of $BaSO_4$ of 0.08 wt% and 0.1 wt%.

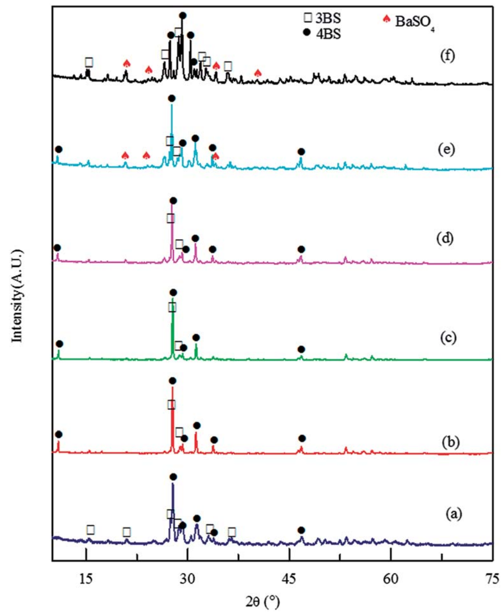

Fig. 1 XRD patterns of the paste after curing with $BaSO_4$ dosages of (a) 0 wt%, (b) 0.02 wt%, (c) 0.04 wt%, (d) 0.06 wt%, (e) 0.08 wt%, and (f) 0.1 wt%.

The mass content of metallic lead in the plate after curing is shown in Table 1. The average content of metal lead was 14.5 ± 1.9 wt% with the addition of $BaSO_4$. It can be seen that the content of metallic lead was higher in comparison with the plate without $BaSO_4$. Hence, it indicated that $BaSO_4$ had a significant influence on the curing of the positive plates.

Meanwhile, $BaSO_4$ also had a significant impact on morphology of plate during the curing, as shown in Fig. 2. The particles aggregated together with the increasing dosage of $BaSO_4$. The aggregation can be attributed to the promotion of the 4BS nucleation density on non-uniform distributed $BaSO_4$, consistent with the XRD analysis.

3.3 The effect of $BaSO_4$ on the formation of positive plate

In contrast to the significant impact of $BaSO_4$ doping on the curing of positive plate, it had different influence on the formation of positive plate, both in term of structure and morphology. The active mass consisted of β-PbO_2 and $PbSO_4$, and was dominated by β-PbO_2, which can be seen from Fig. 3. The average content of lead dioxide was 92.1 ± 1.1 wt% in the presence of $BaSO_4$, and 94.1 wt% in the absence of $BaSO_4$, as

Table 1 The content of metallic lead in PAM after curing process

The dosage of $BaSO_4$ (wt%)	0	0	0	0.02	0.04	0.06	0.08	0.1
The content of metallic Pb (wt%)	7		7.2	15.0	11.4	16.7	15.2	14.4

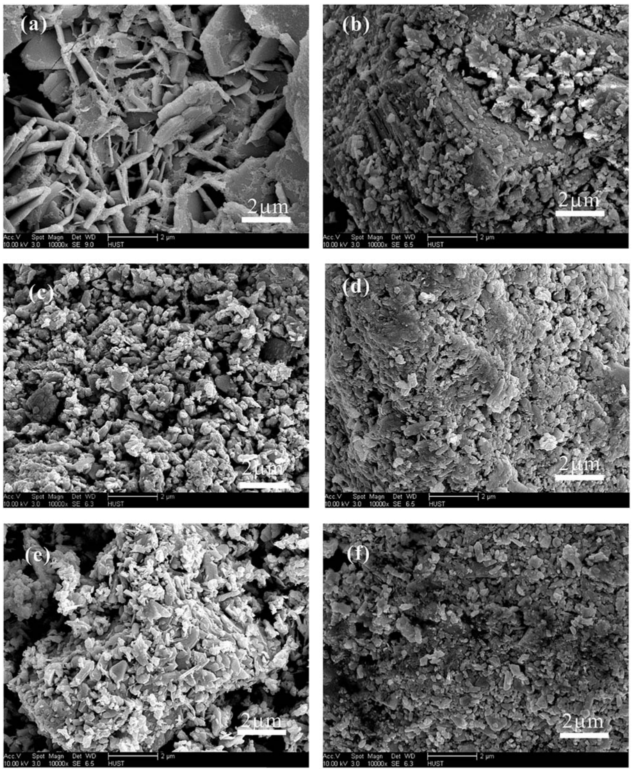

Fig. 2 SEM images of cathode plates after curing with $BaSO_4$ dosages of (a) 0 wt%, (b) 0.02 wt%, (c) 0.04 wt%, (d) 0.06 wt%, (e) 0.08 wt%, and (f) 0.1 wt%. The acceleration voltage was 10 kV and the spot size was 3 during SEM image acquisition.

summarized in Table 2, indicating that $BaSO_4$ had negligible impact on the content of lead dioxide during formation. As can be seen from Fig. 3, the phase of PAM after formation procedure

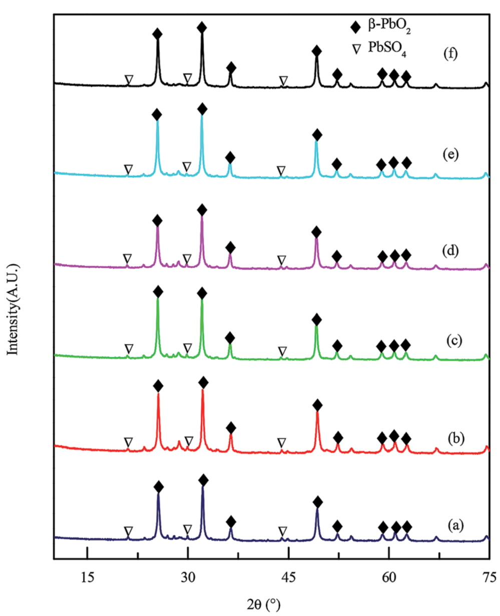

Fig. 3 XRD patterns of the active mass with $BaSO_4$ dosages of (a) 0 wt%, (b) 0.02 wt%, (c) 0.04 wt%, (d) 0.06 wt%, (e) 0.08 wt%, and (f) 0.1 wt%.

Table 2 The content of lead dioxide in PAM after formation process

The dosage of $BaSO_4$ (wt%)	0	0.02	0.04	0.06	0.08	0.1
The content of PbO_2 (wt%)	94.1	92.9	90.9	92.2	93.4	91.0

consisted of β-PbO_2 and $PbSO_4$, and the predominant crystal phase was β-PbO_2.

The morphology after formation is shown in Fig. 4. As can be seen from the photo of the plates in Fig. 4(a), there was no significant change on the surface of plates with varied dosage of $BaSO_4$, with some white dots distributed on the surface of these plates. However, $BaSO_4$ had a dramatic impact on the microstructure of the PAM in the formation process. The particles in PAM became more agglomerated with the increasing dosage of $BaSO_4$, which was in line with the aggregation of 4BS after the curing process.

3.4 The effect of $BaSO_4$ on the battery performance

After curing and formation process, the plates were assembled to a battery to evaluate the effect of $BaSO_4$ on the performance of lead acid battery. The 1C discharge time is shown in Fig. 5 for the testing batteries with different dosage of $BaSO_4$. The 1C discharge time was 47 min in the absent of $BaSO_4$, which was quite similar with that in the presence of $BaSO_4$, and the average discharging time was 43.6 ± 0.7 min. This indicated that $BaSO_4$ did not exhibit evident negative impact on the large current discharge performance of the battery.

The 20 h rate of the testing batteries was evaluated with different dosage of $BaSO_4$ added in the plate, as can be seen from Fig. 5. The 20 h rate of all batteries remained at about 2 A h with the increasing dosage of $BaSO_4$, and it could be found that the 20 h rate achieved 2.46 A h in the presence of 0.1% $BaSO_4$, and the average mean capacity was 2.1 ± 0.3 A h. It was clear the 20 h rates of the batteries in the presence of $BaSO_4$ were lower than the batteries in the absent of $BaSO_4$ (2.78 A h). Hence, the addition of $BaSO_4$ had remarkable influence on the 20 h rate of all the batteries.

The change of the 10 h capacity retention rate of the testing batteries with different dosages of $BaSO_4$ added in the plate is presented in Fig. 5, where C_0 is the rated 10 h rate capacity of the battery, and C_n is the n times of 10 h rate capacity of the battery. The capacity retention ratios of all batteries with $BaSO_4$ remained at about 80% before 25 cycles, and drops to below 80% in the subsequent cycles. In contrast, the battery in the absence of $BaSO_4$ worked very well during all of 46 cycles. When the capacity retention ratio decreased from 0.8 to 0.6, the cycle stability of batteries deteriorated with the increasing dosage of $BaSO_4$, which indicated that $BaSO_4$ had a negative effect on the cycle stability of the battery. When the capacity retention ratio decreased further from 0.6 to 0.3, the capacity decreased with the increasing dosage of $BaSO_4$, but the cycle stability curve stayed the same when the dosage varies from 0.04 wt% to 0.08 wt%. The battery stability curve indicated that $BaSO_4$ had a severe negative effect on the performance of the battery.

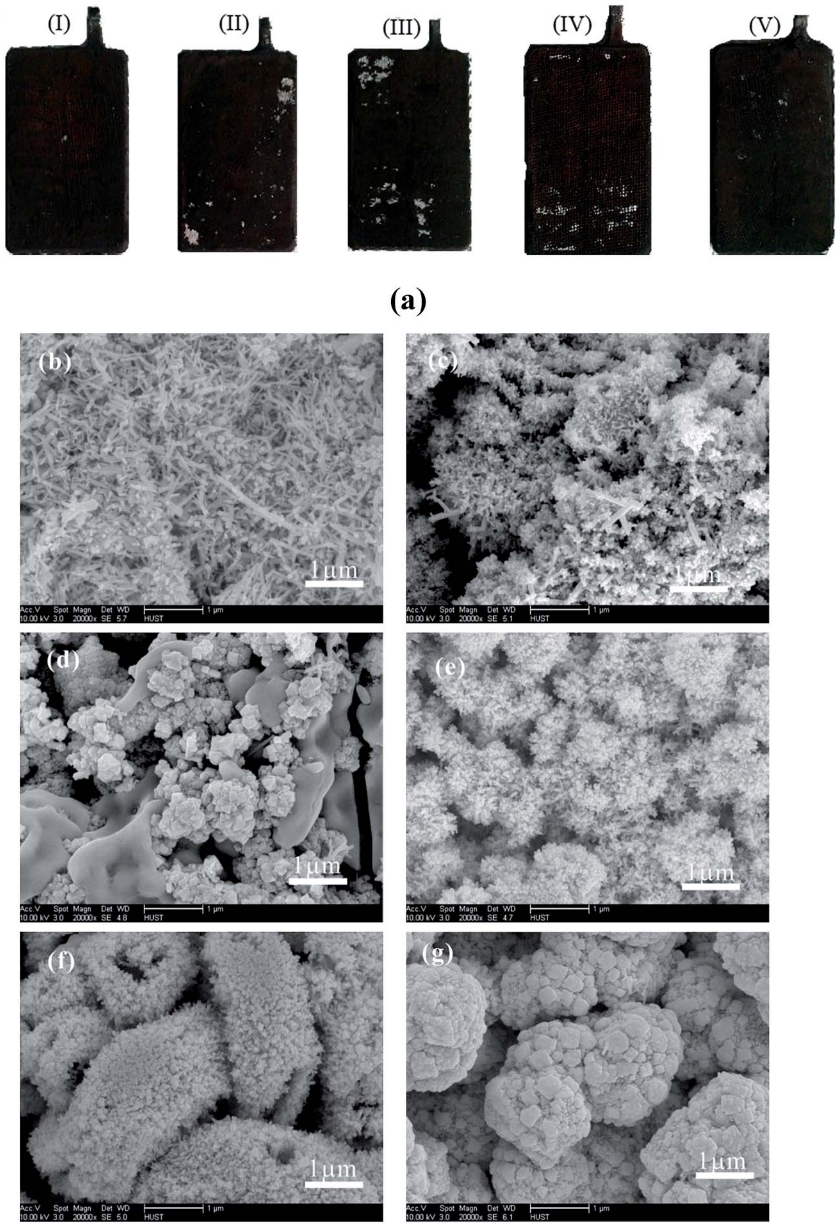

Fig. 4 (a) Photos of the active mass after formation with different dosages of $BaSO_4$, where (I)–(V) denotes for the theoretical addition of 0.02 wt%, 0.04 wt%, 0.06 wt%, 0.08 wt%, and 0.1 wt% $BaSO_4$; SEM images of the active mass with $BaSO_4$ dosage of (b) 0 wt%, (c) 0.02 wt%, (d) 0.04 wt%, (e) 0.06 wt%, (f) 0.08 wt% and (g) 0.1 wt%. The acceleration voltage was 10 kV and the spot size was 3 during SEM image acquisition.

The battery testing with $BaSO_4$ demonstrated an overall tendency that the capacity retention ratio decreased with the increasing dosage of $BaSO_4$. This was different from the previous study that the addition of $BaSO_4$ as electrolyte additive can improve the performance of the battery.[21] As discussed previously, $BaSO_4$ acted as nucleuses to promote nucleation density of lead oxide on top and consequently led to severe aggregation of particles on non-uniform distributed $BaSO_4$ particles. So severe non-uniformity was developed during charging and discharging cycles, and the growing internal stress finally undermined the mechanical integrity of positive plate and causes expansion and shedding-off of PAM on the positive plate, which eventually led to the failure of these batteries.

3.5 Chemical compositions of positive plates of dismantled batteries

After charging and discharging for 46 cycles, the batteries were dismantled after the final charging procedure. The content of $PbSO_4$ and PbO_2 in the positive plate is listed in Table 3. The average content of PbO_2 was 60.5 ± 4.5 wt%, with the highest level found in the sample with 0.1 wt% of $BaSO_4$, which indicated that sulfation was not the primary reason for the failure of batteries. This was supported by the low S content after

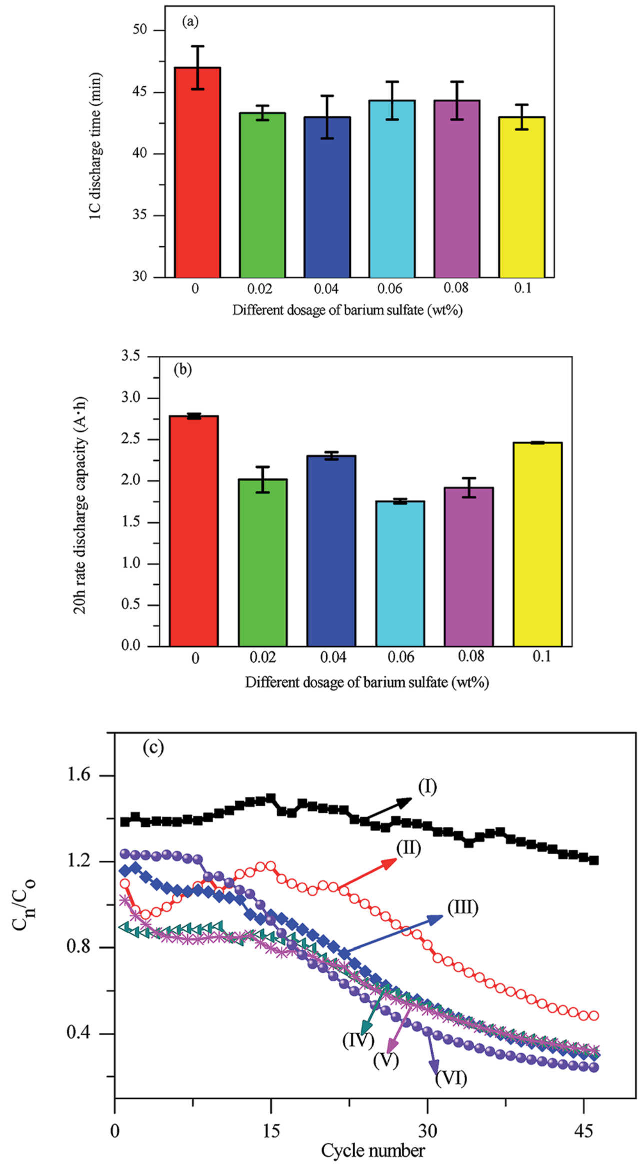

Fig. 5 The 1C discharge time in the discharge current of 2 A (a) and 20 h rate of the battery with different dosage of $BaSO_4$ (b); the capacity retention ratio of battery with various dosage of $BaSO_4$ (c), where (I)–(VI) denotes for the theoretical addition of 0 wt%, 0.02 wt%, 0.04 wt%, 0.06 wt%, 0.08 wt%, and 0.1 wt% $BaSO_4$.

Table 3 The content of $PbSO_4$ and PbO_2 in PAM, and acid density in the disassembled batteries after failure[a]

Symbol	Content of PbO_2 (wt%)	Content of $PbSO_4$ (wt%)	Acid density (g cm^{-3})
Ba-0.02	71.0	39.0	1.23
Ba-0.04	60.3	31.2	1.27
Ba-0.06	63.2	37.8	1.32
Ba-0.08	52.7	42.3	1.29
Ba-0.10	63.6	27.5	1.21

[a] Ba-x stands for the theoretical addition of $BaSO_4$ is x% in weight percent.

Table 4 The content of sulfur in PAM after formation and failure

The dosage of $BaSO_4$ (wt%)	0.02	0.04	0.06	0.08	0.1
The content of S after formation (wt%)	0.75	0.96	0.83	0.70	0.95
The content of S after failure (wt%)	3.06	4.19	3.89	5.00	3.85

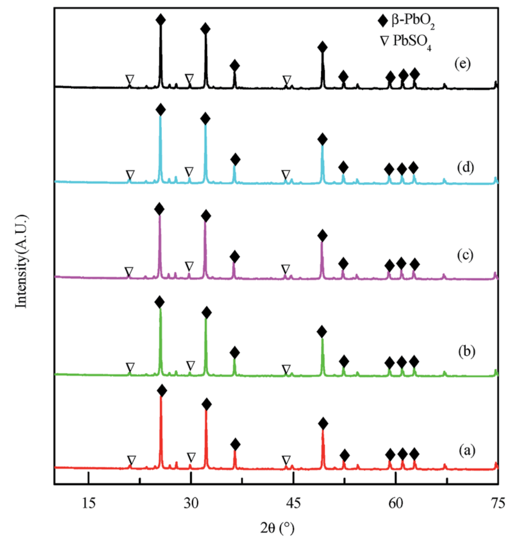

Fig. 6 XRD patterns of the active mass after failure with the dosage of $BaSO_4$: (a) 0.02 wt%, (b) 0.04 wt%, (c) 0.06 wt%, (d) 0.08 wt%, and (e) 0.1 wt%.

formation (in Table 4). The XRD analysis also confirmed that the dominant crystalline phase in the dismantled paste was PbO_2, and a small amount of $PbSO_4$ was also identified at the end of charging procedure (in Fig. 6). Considering that PbO_2 was the dominant phase in dismantled batteries and the content of S was not high after failure, the sulfation was not the dominant reason for the failure of these batteries. This is different from the widely accepted interpretation on the failure of conventional lead acid batteries.[7,22–24]

To examine the failure of lead acid batteries using $BaSO_4$ doped lead oxide as PAM, optical photos and SEM images of the dismantled paste at the 47th battery cycles were acquired. From the optical photos of dismantled positive plates after failure as presented in Fig. 7(a), significant fracture and shedding of PAM were observed. This was believed to be the primary reason for the failure of these batteries in the present of $BaSO_4$. As shown in the microstructure images in Fig. 7(b), the aggregation of active material particles appeared more and more evident with the increase of $BaSO_4$ content. This observation confirmed the hypothesis that the failure of battery was mostly due to the accumulation of internal stress because of the inhomogeneous growth of lead oxide on $BaSO_4$ nucleus during cycled charge and discharge processes.

The content of $BaSO_4$ during the whole process is shown in Fig. 8. The dosage of $BaSO_4$ in lead oxide was measured by ICP

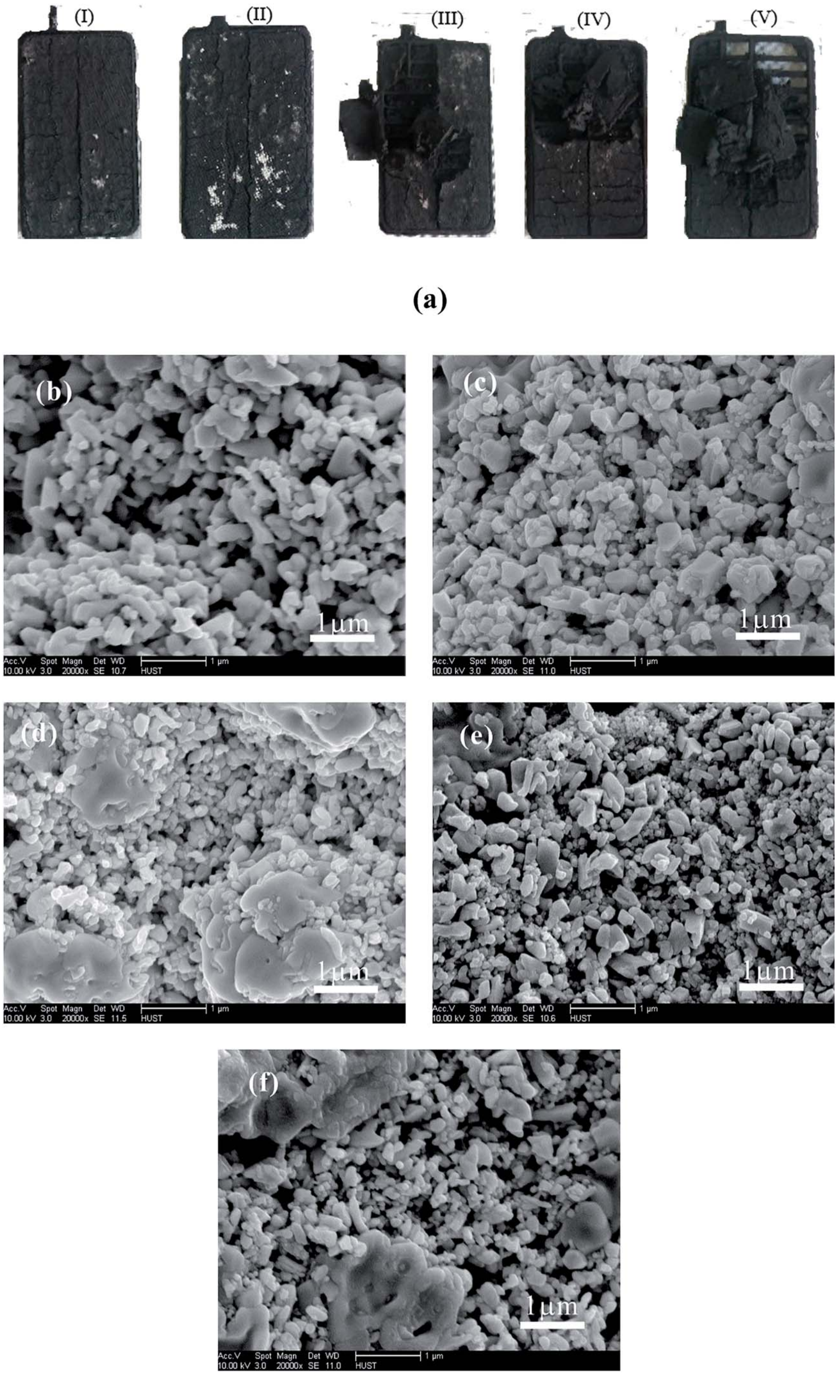

Fig. 7 (a) Photos of the active mass after failure with different dosage of $BaSO_4$, where (I)–(V) denotes for the theoretical addition of 0.02 wt%, 0.04 wt%, 0.06 wt%, 0.08 wt%, and 0.1 wt% $BaSO_4$; SEM images of the active mass after failure with $BaSO_4$ dosage of (b) 0.02 wt%, (c) 0.04 wt%, (d) 0.06 wt%, (e) 0.08 wt% and (f) 0.1 wt%. The acceleration voltage was 10 kV and the spot size was 3 during SEM image acquisition.

and the result was close to the theoretical content, which clearly implied that the quantification method was consistent. The relative portion of barium sulfate *versus* the mass of battery plate appeared to vary significantly at various fabrication stages in Fig. 8 and this was solely attributed to the mass variation of lead containing compound, dominated by $PbSO_4$ during curing, PbO_2 during formation, and mixture of $PbSO_4$ and PbO_2 after failure. In fact the absolute mass of barium sulfate stayed in the plate at various stages and the loss due to its dissolution in the electrolyte was negligible. This indicated that $BaSO_4$ remained in PAM of the plates during the whole process since $BaSO_4$ was insoluble in the sulfuric acid electrolyte. The content of $BaSO_4$ after battery failure was lower than after formation of positive plate as a result of mass increase due to partial transformation of lead dioxide to lead sulfate.

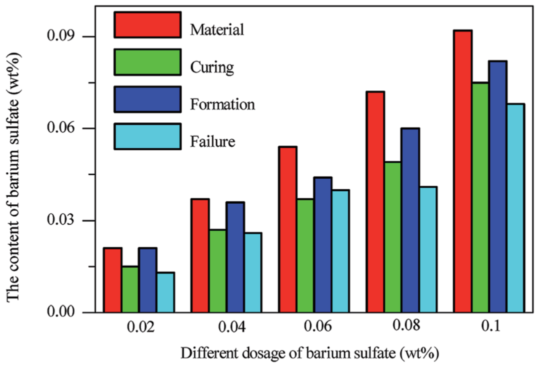

Fig. 8 The content of $BaSO_4$ in the battery during the whole procedure. Material refers to the content of $BaSO_4$ in raw lead oxide; curing, formation, failure refer to the samples after curing, formation and failure of battery.

4 Conclusions

The effect of $BaSO_4$ impurities on the microstructural characteristics of ultrafine lead oxide and the performance of lead acid battery made from these lead oxide were investigated. Ultrafine lead oxide was prepared *via* low temperature calcination of lead citrate, and novel lead acid batteries were assembled using this material.

The presence of $BaSO_4$ impurities demonstrated dramatic influence on the crystalline phase of the positive plates during curing, of which the highest content of metallic lead was 16.7% with the $BaSO_4$ dosage of 0.06%. It also showed a drastic effect on the morphology, resulting in severe particles aggregation with the increasing dosage of $BaSO_4$. The presence of $BaSO_4$ had negligible effect on the crystalline phase of the positive plates during formation, but the morphology analysis indicated that the active mass particle became strongly aggregated with the increasing dosage of $BaSO_4$. $BaSO_4$ also had a significant negative effect on charge/discharge cycles with 100% DOD, which can be attributed to the expansion and shedding of active mass. The non-uniform growth of lead oxide on $BaSO_4$ nucleus and accumulation of internal stress were proposed to be the primary reasons for the failure of batteries through the analysis of the dismantled spent batteries. This study also provides useful guidance on impurities control during the recovery of spent lead paste through hydrometallurgical process.

Acknowledgements

The authors thank for the financial supports from the National Science-technology Support Plan Projects (2014BAC03B02), key project of Hubei Provincial Natural Science Foundation (2014CFA109, 2015CFA133), the Wuhan Planning Project of Science and Technology, China (2013060501010168, 2013011801010593, 2014030709020313 and 2015070404010200), and Innovative and Interdisciplinary Team at HUST (0118261077). The authors would like to thank the Analytical and Testing Center of Huazhong University of Science and Technology for providing the facilities to fulfill the experimental measurements. The technical supports from Wuhan Changguang Power Sources. Co. Ltd., is also gratefully acknowledged. The assistance from Mr Anxu Sheng during electrode preparation and battery assembly, and Dr Bingchuan Liu during manuscript preparation are acknowledged.

References

1 C. R. Cherry, J. X. Weinert and Y. Xinmiao, *Transport. Res. Transport. Environ.*, 2009, **14**, 281–290.
2 H. Y. Chen, L. Wu, C. Ren, Q. Z. Luo, Z. H. Xie, X. Jiang, S. P. Zhu, Y. K. Xia and Y. R. Luo, *J. Power Sources*, 2001, **95**, 108–118.
3 Y. Chang, X. X. Mao, Y. F. Zhao, S. L. Feng, H. Y. Chen and D. Finlow, *J. Power Sources*, 2009, **191**, 176–183.
4 T. W. Ellis and A. H. Mirza, *J. Power Sources*, 2010, **195**, 4525–4529.
5 A. Poullikkas, *Renewable Sustainable Energy Rev.*, 2013, **27**, 778–788.
6 X. Tian, Y. Gong, Y. F. Wu, A. Agyeiwaa and T. Y. Zuo, *Resour., Conserv. Recycl.*, 2014, **93**, 75–84.
7 L. T. Lam, N. P. Haigh, C. G. Phyland and A. J. Urban, *J. Power Sources*, 2004, **133**, 126–134.
8 M. A. Kreusch, M. J. J. S. Ponte, H. A. Ponte, N. M. S. Kaminari, C. E. B. Marino and V. Mymrin, *Resour., Conserv. Recycl.*, 2007, **52**, 368–380.
9 A. Zabaniotou, E. Kouskoumvekaki and D. Sanopoulos, *Resour., Conserv. Recycl.*, 1999, **25**, 301–317.
10 E. Sayilgan, T. Kukrer, G. Civelekoglu, F. Ferella, A. Akcil, F. Veglio and M. Kitis, *Hydrometallurgy*, 2009, **97**, 158–166.
11 N. K. Lyakov, D. A. Atanasova, V. S. Vassilev and G. A. Haralampiev, *J. Power Sources*, 2007, **171**, 960–965.
12 X. F. Zhu, X. He, J. K. Yang, L. X. Gao, J. W. Liu, D. N. Yang, X. J. Sun, W. Zhang, Q. Wang and R. V. Kumar, *J. Hazard. Mater.*, 2013, **250**, 387–396.
13 J. Q. Pan, Y. Z. Sun, W. Li, J. Knight and A. Manthiram, *Nat. Commun.*, 2013, **4**, 2178.
14 L. Li, X. F. Zhu, D. N. Yang, L. X. Gao, J. W. Liu, R. V. Kumar and J. K. Yang, *J. Hazard. Mater.*, 2012, **203**, 274–282.
15 D. N. Yang, J. W. Liu, Q. Wang, X. Q. Yuan, X. F. Zhu, L. Li, W. Zhang, Y. C. Hu, X. J. Sun, R. V. Kumar and J. K. Yang, *J. Power Sources*, 2014, **257**, 27–36.
16 X. J. Sun, J. K. Yang, W. Zhang, X. F. Zhu, Y. C. Hu, D. N. Yang, X. Q. Yuan, W. H. Yu, J. X. Dong, H. F. Wang, L. Li, R. V. Kumar and S. Liang, *J. Power Sources*, 2014, **269**, 565–576.
17 D. Pavlov, P. Nikolov and T. Rogachev, *J. Power Sources*, 2010, **195**, 4435–4443.
18 H. Vermesan and N. Hirai, *Rev. Chim.*, 2007, **58**, 1221–1225.
19 K. Sawai, T. Funato, M. Watanabe, H. Wada, K. Nakamura, M. Shiomi and S. Osumi, *J. Power Sources*, 2006, **158**, 1084–1090.
20 H. Vermesan, N. Hirai, M. Shiota and T. Tanaka, *J. Power Sources*, 2004, **133**, 52–58.
21 H. Karami and A. Yaghoobi, *J. Cluster Sci.*, 2010, **21**, 725–737.
22 J. H. Yan, W. S. Li and Q. Y. Zhan, *J. Power Sources*, 2004, **133**, 135–140.
23 M. Saravanan and S. Ambalavanan, *Eng. Failure Anal.*, 2011, **18**, 2240–2249.
24 Y. L. Guo, S. Q. Tang, G. Meng and S. J. Yang, *J. Power Sources*, 2009, **191**, 127–133.

